A high energy phase retarder for the simultaneous production of right- and left-handed circularly polarized x rays

C. T. Venkataraman, J. C. Lang, C. S. Nelson, G. Srajer, D. R. Haeffner, and S. D. Shastri
Advanced Photon Source, Argonne National Laboratory, Argonne, Illinois 60439

(Received 4 December 1997; accepted for publication 6 February 1998)

We have fabricated and characterized the performance of a monolithic Ge Bragg–Laue phase retarder capable of simultaneously producing both right- and left-handed circularly polarized x rays. The energy range of operation of the phase retarder is between 50 and 100 keV making it well suited to the measurement of spin-dependent Compton profiles within the impulse approximation, primarily because of the increased momentum resolution and larger Compton scattering cross section available at these higher incident energies. Although the phase retarder was optimized for operation at 86 keV, it can produce highly circularly polarized x rays over a substantial energy range. The performance of the phase retarder was tested via magnetic Compton scattering measurements on an Fe sample at the undulator A of the Advanced Photon Source. It was found to perform well in terms of flux and degree of circular polarization thereby greatly reducing the data collection times required for this inherently weak scattering process. © *1998 American Institute of Physics.* [S0034-6748(98)01005-3]

I. INTRODUCTION

Synchrotron radiation sources have made possible the measurement of spin-dependent momentum distribution of electrons with hard x rays. Rendering these experiments feasible, however, requires an x-ray source with high flux density, high degree of circular polarization, and high stability of the polarization state. Furthermore, an x-ray source that is tunable over a wide energy range and has the ability to rapidly reverse the photon helicity greatly extends the range of possible experiments. Circularly polarized (CP) x rays have until now been produced essentially in three ways: (i) use of perfect crystal x-ray phase retarders (XPRs), (ii) selection of synchrotron radiation off-axis to the orbital plane, and (iii) specialized insertion devices, such as elliptical multipole wigglers (EMWs). While each technique has its specific benefits, high energy phase retarders coupled with a planar undulator have proved to be versatile, simple to operate, economical to fabricate, and extremely successful at energies below 100 keV. Although they may not match a focused EMW beam in throughput flux at these higher energies,[1] they do provide other distinct advantages. Because they are the last optical element prior to the sample, the final photon polarization state is well defined and not subject to the instabilities of the particle orbit. Helicity switching can be incorporated, thus reducing beam-related errors in the low count-rate signal. They can be well matched to other optical elements such as high-energy analyzers to obtain higher momentum resolution crucial to the current developments in the measurement of spin-dependent Compton profiles. Finally, their performance is enhanced at lower beam emittances, which is one of the features currently available at third-generation synchrotron sources.

Previous XPRs used to produce high energy (>20 keV) CP x rays have utilized both reflection and transmission Laue geometries.[2–4] The XPR described in this article is of a monolithic design using both Bragg and Laue reflections to monochromatize and polarize the x-ray beam. It is an upgrade from our previous design in that both the left- and right-handed beams are simultaneously excited.[3] The two emerging CP beams are spatially separated by only a few mm and are parallel to the incident beam. This provides good dispersive matching to enhance the throughput and allows for the incorporation of rapid helicity switching.

II. BRAGG–LAUE X-RAY PHASE RETARDER

The principle behind an XPR is the four-refringent property of a perfect single crystal in a transmission geometry as described by dynamical diffraction theory. At the Brillouin zone boundary, four wavefields propagate through the crystal corresponding to the two polarizations of the α and β branches.[2,4,5] The two polarization states, σ and π, perpendicular and parallel to the diffraction plane, respectively, propagate through the crystal with different phase velocities. The relative phase difference between the two polarization states depends on the deviation from the Bragg condition. At the exact Bragg condition, at the exit face of a crystal of thickness t, this relative phase difference is given by

$$\phi = \frac{t r_e \lambda |F_H| (1 - |\cos 2\theta_B|)}{V \cos \theta_B},$$

where r_e is the classical electron radius, λ is the incident x-ray wavelength, V is the unit cell volume, F_H is the structure factor specific to the reflection, and θ_B is the Bragg angle. When the amplitudes of the two components are equal and their phase shift is $\pm(2n+1)\pi/2$, they combine to produce circularly polarized x rays. Therefore, for a given crystal thickness, the degree of circular polarization of the emerging beams is a function of the incident energy.

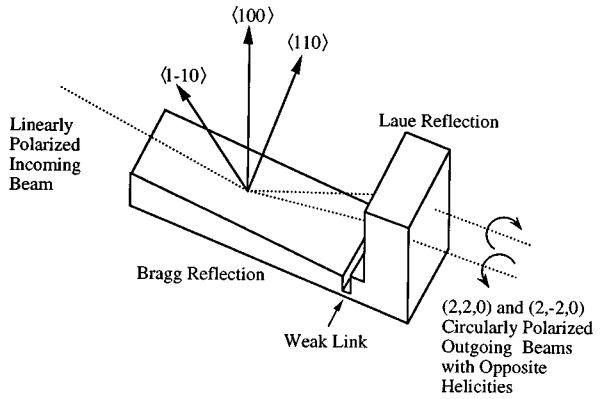

FIG. 1. The high energy x-ray phase retarder. The XPR is fabricated from an oriented (100) Ge boule. The incident beam undergoes successive Bragg and Laue reflections after which it is circularly polarized. The weak link that allows rotation of the Laue portion with respect to the Bragg is indicated.

Hirano and co-workers have also suggested a crystal optic design that allows for rapid helicity reversal.[4] This design utilizes a conventional double-crystal monochromator and a forward diffracted Laue reflection. The Laue crystal is oriented such that either the (220) or (2-20) reflections can be excited through the rotation of only a few arcminutes. Because these reflections are crystallographically equivalent and perpendicular, they can produce right or left CP x rays, respectively. Furthermore, utilizing the forward diffracted beam leaves the direction of the outgoing beam unchanged upon helicity reversal. This phase retarder, however, has one major drawback compared with the monolithic Bragg–Laue design. The dispersive geometry between the Bragg monochromator and the Laue reflections results in an order of magnitude loss in outgoing flux.

In the current design, the Bragg–Laue XPR is a germanium (Ge) monolith cut from an oriented Ge (100) single-crystal boule. It comprises a Bragg section with a [100] surface normal and a Laue section where symmetric (220) planes polarize the beam in a transmission geometry (Fig. 1). The asymmetry angle for this scattering geometry for the (220) planes is 0.35° in the diffraction plane. This arises from a 1.7° miscut of the crystal surface with respect to the [001] direction and is provided so that the Bragg-reflected beam can exit the crystal surface.

This design is a modification of previous Bragg–Laue monolithic XPRs,[2,3,6] which had the surface normal of the Bragg portion of the crystal oriented along the [110] direction. To obtain CP x rays, the phase retarder plane of diffraction had to be oriented at $\pm\pi/4$ with respect to the synchrotron orbital plane. To obtain helicity reversal, the whole XPR had to be rotated by 90° about the incident beam, which was cumbersome and could not be done rapidly.

The XPR described here retains the nondispersive nature of the monolithic design and also provides the capability for rapid helicity reversal. The whole optical element is 79 mm long, which results in a 5 mm separation of the (220) and (2-20) beams at the exit face. The thickness of the Laue portion is 14.81 mm, which is optimal for operation at 86 keV. This energy was chosen considering the output flux of the undulator and the applicability to magnetic Compton scattering measurements. Furthermore, at 86 keV, the incident energy is below the lead (Pb) K absorption edge. This minimizes the resulting fluorescence from the Pb shielding that could otherwise contaminate the Compton peak. The XPR is, however, capable of producing CP x rays, with a lower degree of circular polarization, over a range of energies from 50 to 100 keV, making it more versatile in application. This is significant as the cross section for magnetic Compton scattering increases with incident energy and with degree of circular polarization. Because the magnetic Compton cross section is inherently weak (soft ferromagnets, e.g., Fe, only produce a magnetic effect of 1%–2%), an increase by a factor of about 3 gained from 20 to 80 keV incident energy for a specific scattering geometry can significantly accelerate data acquisition times.

The advantage of fabricating the XPR from Ge over silicon (Si) has been discussed previously.[2,3] In brief, Ge outperforms Si in its ability to polarize the incident x rays because it absorbs more of the β branch wavefields, which tend to cancel out the polarization produced by the α wavefields.

The linearly polarized incident white beam undergoes successive Bragg and Laue (220) reflections. The length of the Bragg portion is determined by the resulting footprint at grazing incidence. By spreading out the beam over a wide area and providing contact cooling, the heat load on the crystal is reduced. In this orientation, the (220) planes are at $\pm\pi/4°$ to the orbital plane. The two beams pass though the Laue portion of the XPR and emerge from the exit face circularly polarized, with opposite helicities, and parallel to each other and to the incident beam. In this manner, dispersion matching is achieved. The Laue and Bragg diffraction conditions differ by less than an arcsecond in angle due to differing indices of refraction for the two geometries. To compensate for this, a weak link is cut between the two parts so that the Laue portion can be rotated with respect to the Bragg.

III. EXPERIMENTAL SETUP

The performance of the XPR was measured through a magnetic Compton scattering experiment on a polycrystalline Fe sample. Because the magnetic moment of Fe is well known, one can use the measured magnetic Compton cross section to extract the degree of circular polarization, P_C. Incident radiation from both an undulator A insertion device (ID) and a bending magnet (BM) source at the Advanced Photon Source (APS) were used to characterize the XPR in terms of P_C and throughput efficiency. A schematic of the experimental setup is given in Fig. 2. Aluminum and copper filters were placed in the incident beam to absorb the low-energy radiation. This served the dual purpose of reducing the scattered background and reducing the heat load on the crystal. White-beam slits far upstream of the XPR served to collimate the incident beam. A second set of tungsten white-beam slits placed just before the XPR further defined the incident beam and reduced the scatter around the XPR. The XPR was mounted on a microstepped double-arc goniometer to provide rotations about a horizontal axis perpendicular to the incident beam, which defines the Bragg angle, and about the beam direction. These arcs were in turn mounted on a

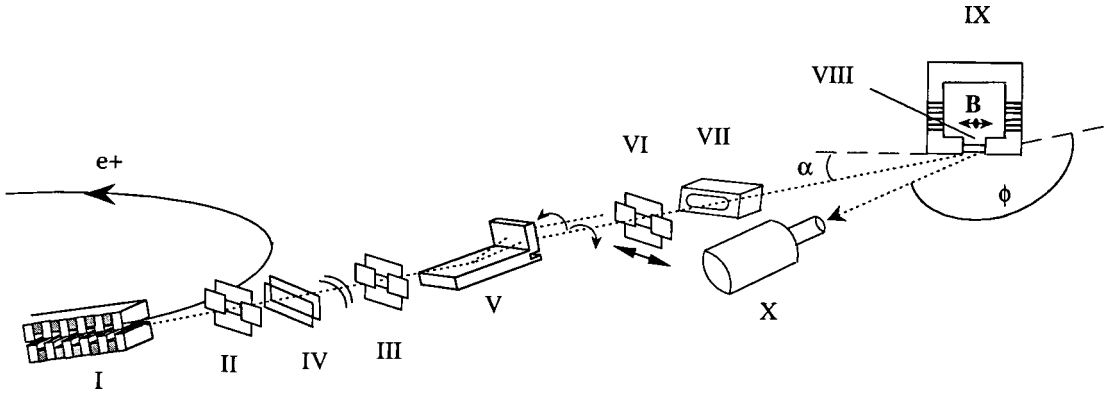

FIG. 2. The experimental setup for the characterization of P_C of the XPR through a magnetic Compton scattering measurement. White radiation from an undulator or bending magnet source (I) passes through two white beam slits (II and III) and a series of filters (IV) before it is incident on the Bragg part of the Ge XPR (V). After undergoing successive Bragg and Laue reflections, two CP x-ray beams of opposite helicity are produced. Specific helicity beams are selected by a slit mounted on a translational stage (VI). An ionization chamber (VII) acts as a monitor. The Fe sample (VIII) is placed between the poles of an electromagnet (IX) with reversible magnetic field direction. A Ge solid-state detector (X) collects the scattered radiation, which is analyzed by a multichannel analyzer. The scattering angle, ϕ, was 151.8°; the angle between the magnetic field and the incident beam, α, was 23°. Distances and dimensions are not to scale.

second goniometer to provide rotation about the vertical axis. This last rotation proved crucial in the alignment of the XPR so that both CP x-ray beams had the same energy. Immediately after the XPR, a tungsten beam stop blocked the direct beam. Upon exiting the XPR, a single helicity CP x-ray beam was selected by a slit mounted on a translation stage. The CP x-ray beam then passed through a sealed Ar ionization chamber that served as a beam monitor before the beam was incident on the sample.

The Fe sample was placed in contact between the poles of an electromagnet capable of providing magnetic fields up to 2.5 kG (measured in the air gap). A Ge solid-state detector was used with an energy resolution of 400 eV at 88 keV, and the scattered energies were resolved using a multichannel analyzer. At these high energies, the randomly scattered radiation contributed heavily to the background. Lead $K\alpha$ and $K\beta$ fluorescence arising from the shielding can contaminate the Compton spectrum. Therefore, much care was taken to shield the detector from the broad spectrum of scattered radiation arising from the white beam incident on the XPR.

IV. CHARACTERIZATION OF THE XPR

Magnetic Compton spectra were taken for a series of energies between 55 and 100 keV. The technique used to take the data is essentially the same as described by Yahnke *et al.*[3] with a major improvement in data collection times. The magnetic contribution to the Compton spectra is obtained by taking the difference of the Compton spectra under a reversal of magnetic field. The scattered energy spectra were taken as a series of ABBA sequences, where A and B correspond to the two magnetic field directions. Using the 1-ID undulator source at the APS, each ABBA sequence was set to take about 20 s at a ring current of 90 mA. A total data collection time of 20 min at a count rate of 400 counts/s in the Compton peak was sufficient to clearly determine a difference signal of 1% (Fig. 3). Several such scans could be summed to yield better statistics.

The total double-differential cross section for spin-polarized electrons is given by[7]

$$\frac{d^2\sigma}{d\Omega\, dE'} = \frac{1}{2} r_e^2 \frac{E'}{E_0}\left[f_1 J(p_2) + \left(\frac{E_0}{mc^2}\right) P_C S(\alpha) J_{\mathrm{mag}}(p_z)\right],$$

$$f_1 = 1 + \cos^2\phi + \frac{E_0 - E'}{mc^2}(1-\cos\phi) + P_L \sin^2\phi,$$

$$S(\alpha) = \pm\left[\cos\phi\cos\alpha + \frac{E'}{E_0}\cos(\phi-\alpha)\right](1-\cos\phi),$$

where E_0 and E' are the incident and scattered energies, respectively, ϕ is the scattering angle, α is the angle between the magnetic field and the incident wave vector, and P_L is the component of linear polarization in the incident beam.

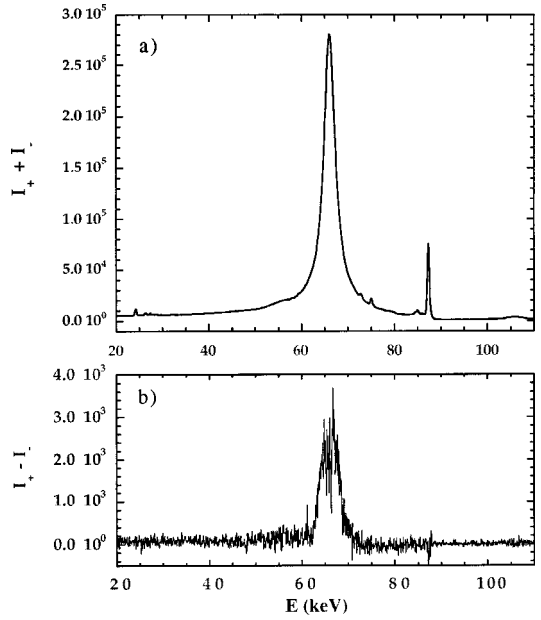

FIG. 3. (a) A typical multichannel analyzer (MCA) spectrum from the Fe sample measured at the APS undulator A beamline. The spectrum shown is the summed signal for the two opposite magnetization directions. The Compton and elastic peaks at 65.6 and 86.5 keV, respectively, are clearly resolved from the highly suppressed Pb fluorescence lines. (b) The difference signal obtained after about 60 min of data collection.

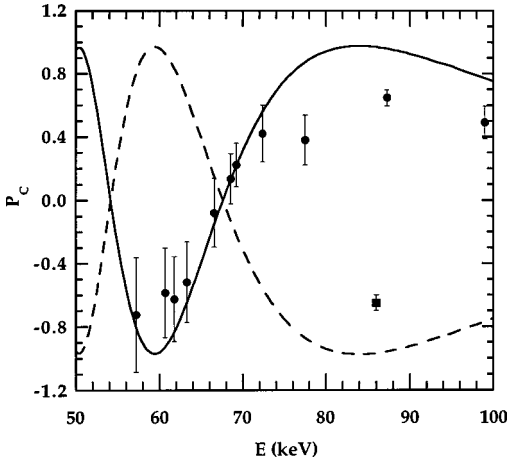

FIG. 4. Comparison of experimental and theoretical P_C produced by the Ge XPR by the (220) reflections at 86.5 keV. The error bars are purely statistical. The two data points at 86 and 86.5 keV are acquired from the two opposite helicity CP x-ray beams. Fine tuning of the alignment of the XPR about the vertical axis is required to ensure that both helicity beams have the same energy.

The $S(\alpha)$ term reverses sign for opposite sample magnetization directions or opposite incident photon helicities. The Compton profiles, $J(p_z)$ and $J_{\mathrm{mag}}(p_z)$, are the projections of the total and magnetic ground state electron momentum densities along the scattering vector. When integrated over the momentum, p_z, they give the total, N_{tot}, and unpaired (magnetic), N_{mag}, Compton scattering electrons, respectively. It can be seen that the dependence of the scattered intensity on the spin-polarized electrons can be isolated by taking the difference of the intensities under either magnetization reversal or helicity reversal. The asymmetry ratio, R, is then calculated from the integrated difference and sum signals and is given by

$$R=\frac{I_+-I_-}{I_++I_-},$$

where I_+ and I_- are the intensities of the Compton spectra for opposing directions of the sample magnetization (or incident photon helicity). The asymmetry ratio is a function of P_C and the scattering geometry,

$$R=\frac{P_C S(\alpha) N_{\mathrm{mag}}}{f_1 N_{\mathrm{tot}}}.$$

For Fe, N_{mag} and N_{tot} were taken as 2.07 and 26 over the range of integration ($-10<p_z<+10$ a.u.), respectively. Therefore, by using the experimentally determined R, one can solve for P_C. It was assumed that there was no unpolarized component to the beam.

Figure 4 gives the experimentally determined P_C as a function of incident energy. While the performance of the XPR does not meet theoretical expectations at higher energies, it is still capable of producing above 65% CP x rays at 86 keV. In addition, both helicity beams yield the same value of P_C within the error bars making helicity switching a viable alternative to magnetization reversal. The larger error bars at lower energies arise from poorer statistics due to shorter data collection times. At lower energies, the XPR has reduced flux throughput through the Laue portion due to the combination of dynamical and filtering effects. The difficulty in reducing statistical error is due to the inherently weak magnetic scattering cross section. To obtain a statistical error of 1% for an R of 1%, it can been calculated that 10^8 counts are required in the integral of the summed spectra. For our initial characterization of the performance of the XPR, we were able to reduce the statistical error at 86 keV to less than 10% in about 1 h of data collection.

The flux output from the XPR was characterized using the 1-BM APS bending magnet calculated to deliver 9.4×10^9 photons/s/0.1% bandwidth (BW) at a ring current of 100 mA (at 85 keV) taking into account all windows, slits, and filters. The flux in the circularly polarized beam, after consecutive (220) Bragg and (220) Laue reflections, was measured to be approximately 2×10^7 photons/s. (For comparison, the flux on the undulator A beamline was approximately 2×10^9 photons/s.) This is an order of magnitude less than the theoretical flux expected from the XPR. The source of this loss is suspected to be strain within the Laue portion of the crystal. The intensities of (400) Bragg and Laue reflections, both measured using the Laue part of the XPR, were compared and the ratio found to be an order of magnitude less than predicted by theory. The crystal does not appear to be undergoing thermal strain as there was no observed rise in the temperature of the crystal with the white beam incident on it. It is likely that the strain is inherent within the Ge single crystal and the 14.1 mm Laue thickness would compound the loss of intensity arising from it. Mechanical strain due to the rotation of the Laue part through the weak link could also be a factor. We plan analytical tests of the XPR to look for sources of strain, such as topographical studies and measurement of rocking curves under strained conditions.

In summary, we have demonstrated the successful performance of a monolithic Ge Bragg–Laue XPR in terms of P_C and throughput efficiency. The simultaneous production of both helicities can be exploited to measure difference signals with a fixed applied magnetic field. Low temperature studies of hard ferromagnets have indicated that helicity switching over magnetic field reversal is the preferred method of obtaining spin-dependent behavior of such systems.[8] To obtain switching frequencies of the order of 1 Hz, a shutter mechanism will need to be incorporated into the current experimental setup. The XPR is currently being applied towards the measurement of spin-dependent momentum distributions of ferromagnetic systems.

[1] J. C. Lang, G. Srajer, and R. J. Dejus, Rev. Sci. Instrum. **67**, 62 (1996).
[2] D. M. Mills, Nucl. Instrum. Methods Phys. Res. A **266**, 531 (1988).
[3] C. J. Yahnke, G. Srajer, D. R. Haeffner, D. M. Mills, and L. Assoufid, Nucl. Instrum. Methods Phys. Res. A **377**, 128 (1994).
[4] K. Hirano, T. Ishikawa, I. Nakamura, M. Mizutani, and S. Kikuta, Jpn. J. Appl. Phys., Part 2 **33**, L689 (1994).
[5] B. W. Batterman and H. Cole, Rev. Mod. Phys. **36**, 681 (1964).
[6] J. A. Golovchenko, B. M. Kinkaid, R. A. Levesque, A. E. Meixner, and D. R. Kaplan, Phys. Rev. Lett. **57**, 202 (1986).
[7] D. M. Mills, Phys. Rev. B **36**, 6178 (1987).
[8] P. K. Lawson, J. E. McCarthy, M. J. Cooper, E. Zukowski, D. N. Timms, F. Itoh, H. Sakurai, Y. Tanaka, H. Kawata, and M. Ito, J. Phys.: Condens. Matter **7**, 389 (1995).